Hierarchical ZIF-8 composite membranes: Enhancing gas separation performance by exploiting molecular dynamics in hierarchical hybrid materials

Salman Shahid [a,c,**], Gino V. Baron [b], Joeri F.M. Denayer [b], Johan A. Martens [c], Lik H. Wee [c,d], Ivo F.J. Vankelecom [c,*]

[a] Centre for Advanced Separations Engineering (CASE), University of Bath, Chemical Engineering Department, Calverton Down, Bath, United Kingdom
[b] Vrije Universiteit Brussel, Department of Chemical Engineering, Pleinlaan 2, B-1050, Brussel, Belgium
[c] Centre of Surface Chemistry and Catalysis, KU Leuven, Celestijnenlaan 200f - Box 2461, 3001, Leuven, Belgium
[d] Department of Chemical Engineering and Biotechnology, University of Cambridge, West Cambridge Site, Philippa Fawcett Drive, Cambridge, CB3 0AS, UK

ARTICLE INFO

ABSTRACT

Mixed matrix membranes (MMM) incorporating metal-organic framework (MOF) fillers have gained increasing attention in addressing environmental and sustainability challenges. Hierarchical materials combining pore sizes of different length scales are expected to facilitate molecular diffusion and mass transfer for the optimization of catalysis and separation processes. Herein, a novel preparation method for hierarchical ZIF-8 (H-ZIF-8) particles is presented for the synthesis of polyimide (PI)-based MMMs with good compatibility between filler and polymer. Gas permeability measurements of polyimide-Matrimid®/H-ZIF-8 MMMs showed 4-fold improvements in permeability of both CO_2 and CH_4 coupled with a marked increase in selectivity and plasticization resistance for MMM with 30 wt% H-ZIF-8 loading. Gas transport analysis in these MMMs revealed that the enhanced gas separation performance of the MMMs can be related to the imidazolate modification of the PI structure and the hierarchical structure of H-ZIF-8, as confirmed by N_2, Ar, mercury porosimetry, SEM, TEM analysis. CO_2 permeability for all MMMs increases with increasing CO_2 concentration and by decreasing temperature. The proof of concept, as demonstrated in this study, could be extended for the preparation of other hierarchical ZIFs and related MMMs.

1. Introduction

Development of energy efficient and environmentally friendly materials and processes has been of great concern for sustainable process applications e.g. energy generation, energy storage, water purification, gas separation and etc. [1]. Membrane-based gas separation has become an attractive technology over traditional separation processes, owing to its low energy consumption, small footprint, no waste generation and easy operation.

During the last two decades, polymeric membranes have been widely explored for the separation of gas mixtures in many industrial applications, such as removal of CO_2 from natural gas, air separation, hydrogen recovery from hydrocarbon mixtures etc. [2–4]. Although various attempts have been devoted to improving the separation performance of promising polymer membranes [5,6], the implementation of polymeric membranes for large-scale industrial high-throughput gas separation processes, however, is still limited, as the majority of the developed polymer membranes have yet to meet the industrial performance standards due to insufficient durability and mechanical stability under actual gas separation conditions and the trade-off between permeability and selectivity [7,8]. For example, the major drawbacks of commercially available glassy polymer membranes (e.g. polyimide (PI)) for natural gas purification are (i) their susceptibility to plasticization, which leads to an undesirable loss in selectivity at high pressures, and (ii) Roberson upper bound limitations due to insufficient CO_2 permeability as polyimide membranes have satisfactory CO_2/CH_4 selectivity.

* Corresponding author.
** Corresponding author. Centre for Advanced Separations Engineering (CASE), University of Bath, Chemical Engineering Department, Calverton Down, Bath, United Kingdom.
E-mail addresses: s.shahid@bath.ac.uk (S. Shahid), ivo.vankelecom@kuleuven.be (I.F.J. Vankelecom).

MMMs comprising of inorganic components, e.g. zeolites [9], carbon materials [10,11] and MOFs [12,13], dispersed in an easily processable polymer matrix provide an alternative option that combines the low cost and easy processability of polymeric materials with the separation performance of inorganic materials [14]. Recently, MOFs, a class of porous hybrid inorganic-organic materials, have drawn huge attention due to their high porosity, adsorption capacity, uniform, and tuneable functionality and pore size [15]. Perez et al. [16] incorporated MOF-5 in a Matrinid® matrix for the separation of CO2/CH4 mixture. The 30 wt % loading MMM showed an increase of 120% in pure gas permeability but this increase was associated with interfacial voids between MOF and polymer matrix. In other studies, Cu-4,4′-bipyridine–hexafluorosilicate (Cu-BPY-HFS) and $Cu_3(BTC)2$ were embedded in a Matrinid® polymer matrix [17,18]. In both studies, enhanced gas permeability was observed with slight decrease in selectivity than the unfilled polymer. Bipyridine based UiO-67 and UiO-66-NH_2 were incorporated in Matri-mid® polymer to enhance the facilitated transport mechanism and resulting MMMs showed a significant increase in gas permeability with slight reduction in selectivity compared to pristine Matrinid® mem-branes [19,20]. In the last decade, the incorporation of ZIFs into a polymer matrix has also been intensively studied [13,18,21–27]. Earlier work of Ordonez et al. [21] studied the ZIF-8 MMMs to investigate molecular separation of gas mixtures (H_2/CO_2 and CO_2/CH_4). Among more recent works include representative work of Song et al. [26] who studied the as synthesized non-dried ZIF-8 based MMMs and showed much better compatibility with the polymer matrix compared to previ-ously reported ZIF-8. Shahid et al. studied surface functionalization of Matrinid® and ZIF-8 filler to enhance the filler dispersion and compatibility [24]. Roberto et al. reported that PEG-200 enhanced the dispersion of non-dried ZIF-8 in MMMs and resulted in excellent CO_2/CH_4 separation performance [27]. Most recently, Machiel et al.

magnetically aligned m-ZIF-8 to enhance enriched pathways of m-ZIF-8 through Matrinid® that showed an increase in CO2 diffusivity with no loss in ideal selectivity [28].

However, a large proportion of the reported studies on MOF-MMMs concern the functional performance alone, focusing predominantly on selective adsorption or diffusion that governs the permselectivity of MMMs [12,15]. So far, almost all reported MOF-MMM systems used microporous MOFs (pore size <2 nm) [15], which does not allow for fast mass diffusion and transfer, limiting their utilization [29]. Therefore, MOFs with hierarchical arrangements of macropores, mesopores, and micropores in a single crystal are desirable for fast mass transportation. MOFs with mesoporosity outmatch microporous MOFs in practice because of their higher pore volumes [30] that offer them more tunable pores in shape and size and diverse nanoscale. Hierarchical MOF ma-terials containing mesopores have shown inherited morphology from MOFs [31] and promising future for application such as catalysis [32], energy storage and conversion [33,34] and gas storage [35]. Yiyin et al. prepared hierarchical HKUST-1 single crystals and well-intergrown mesoporous membrane by etching in homogenous ligand solutions. These hierarchical porous structures significantly improved the CO_2 capture capacity of HKUST-1 by more than 44% at pressures up to 20 kPa [36]. Javier et al. synthesized hierarchal MOF with multichannel pore systems and showed enhanced CO_2 capture capacity [37]. Hierar-chical MOFs have also been studied in separation applications and due to their high tunability control over separation properties can be judi-ciously altered. The liquefied petroleum gas purification has been ach-ieved by engineering the molecular structures of MOFs [38]. [Zn2(btm) 2], a MOF with flexible quasi-discrete pores have been examined for their ability of diffusion and conformation control to purify 1,3-buta-diene (≥99.5%) from butane, butene, and isobutene [39]. With limited applications of hierarchical MOFs for light gas separation these MOFs have never been applied for CO_2/CH_4 separation using MMMs. The objective of the hierarchical (micro- and mesostructured) design is to combine the benefits of smaller intrinsic apertures which will limit the size of molecules that can diffuse into the functional void space thus

providing size selectivity, while the larger mesopore cavity is expected to enhance permeability and selectivity of the MMMs. Herein, the po-tential use of hierarchical ZIF-8 particles as fillers is demonstrated to prepare MMMs (i) with improved binary gas CO_2/CH_4 separation per-formance and (ii) improved plasticization resistance under elevated pressures achieved via polymer surface modification which enhances ZIF-8/polyimide interactions. This is the first study of using hierarchical ZIF-8 particles as fillers to prepare MMMs for CO_2/CH_4 gas separation in comparison to their parent microporous ZIF-8.

2. Experimental section

2.1. Reagents

Matrinid® 5218 PI was supplied by Huntsman, Germany. Zinc ni-trate hexahydrate [$Zn(NO_3)_2$. $6H_2O$] (98%), 2-methylimidazole [$C_4H_6N_2$] (97%) and DMF (99% extra pure) were purchased from Acros Organics, Belgium. All solvents were analytical grade and used without further purification. CO_2, CH_4 and mix (50/50 vol % CO_2/CH_4) gases were supplied by BOC, United Kingdom and used as received (purity 99.999%).

2.2. Synthesis of ZIF-8

ZIF-8 was synthesized via a solvothermal approach, as explained elsewhere [24]. The synthesis mixture contained $Zn(NO_3)_2 \cdot 6H_2O$ (11.75 g) and 2-methylimidazole (25.92 g) in 400 mL of DMF. The so-lution was poured into a 2 L SCHOTT bottle (DURAN) and heated to 140 °C for 4 h. The solid was recovered and washed with DMF through repeated centrifugation and redisperse in an ultrasonic bath. The product was dried in an oven at 80 °C.

2.3. Synthesis of H-ZIF-8

H-ZIF-8 was prepared via an esterification reaction, as explained in our previous work [40]. ZIF-8 (1 g) was pretreated with tert-butanol (50 g) sealed in a stainless steel autoclave and heated at 150 °C with tum-bling for 24 h. The solid was washed with acetone and introduced into an esterification reaction mixture containing oleic acid (1.8 g), glycerol (7.4 g) and tert-butanol (71 g) and treated at 150 °C in a stainless-steel tumbling autoclave for 24 h. The H-ZIF-8 material was recovered by centrifugation and washed with acetone and dried at 80 °C. The sample was activated in a vacuum oven at 150 °C overnight.

2.4. Modification of polymer

The polymer solution was prepared by dissolving 18 wt% Matri-mid®-PI in a 40/60 mixture of dioxane/DMF. The polymer chains were modified by giving them imidazole functionality to make them more compatible with H-ZIF-8. To achieve this, 1-(3-aminopropyl)-imidazole, equivalent to 10 wt% of the polymer, was added to the polymer solution under stirring at 25 °C for 3–4 h. The solution was then precipitated in ethanol to obtain modified PI (M-PI) which was subsequently vacuum dried at 120 °C overnight. The chemical structures of the resulting materials were confirmed by ^{1}H NMR and FT-IR. The degree of modi-fication was evaluated by ^{1}H NMR.

2.5. Preparation of MMMs

The MMM samples were prepared by dispersion casting and solvent evaporation. 10 wt%, 20 wt% and, 30 wt% dried H-ZIF-8 powder was slurried into dioxane/DMF (40/60 wt ratio) for 1 h and then sonicated for 1 h. The suspensions were subsequently stirred for 1 h. The requisite amount of polymer was added slowly in multiple steps. A final 10 min sonication period was then applied, followed by casting on a flat glass plate. The solution was evaporated in a conventional oven at 100 °C for
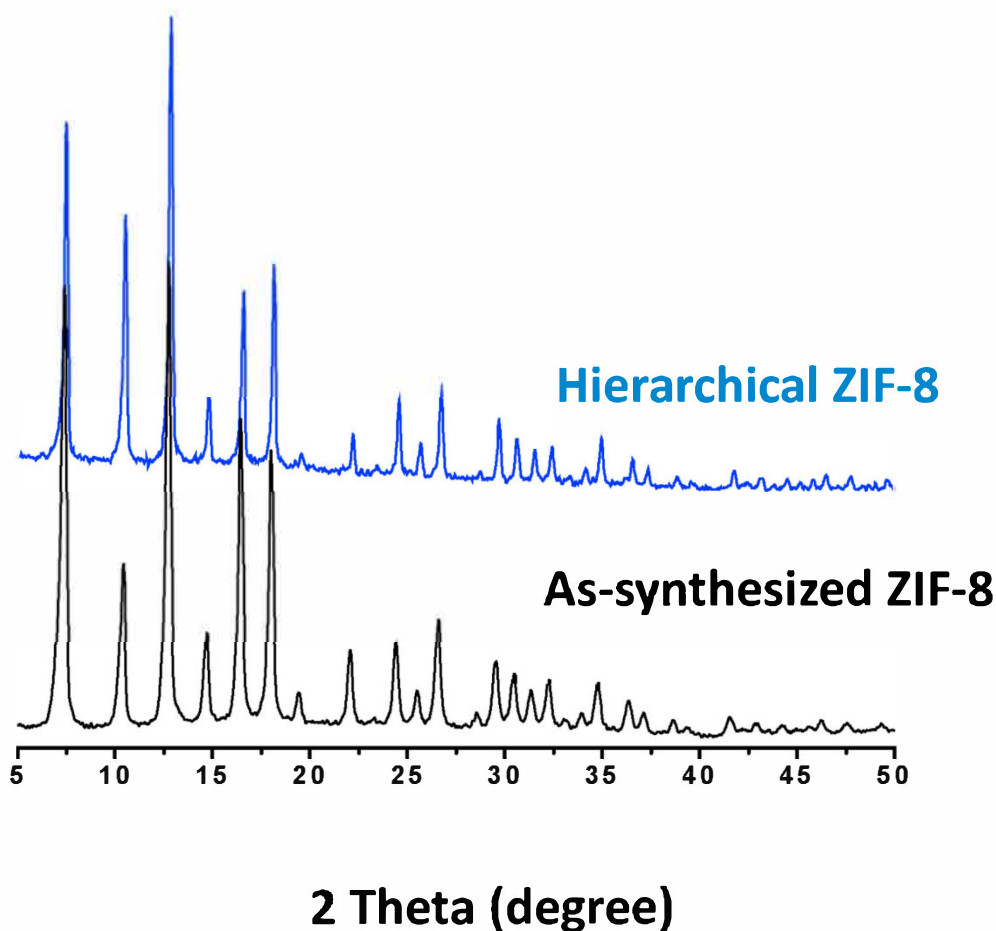
Fig. 1. XRD patterns of ZIF-8 and hierarchical ZIF-8 nanocrystals.

15 h. Subsequently, the membrane was peeled off from the glass plate and annealed to 200 °C at a rate of 20 °C/h and kept at this temperature for 18 h under vacuum and then slowly cooled to room temperature. The same procedure was used to prepare unfilled polymer membranes.

2.6. Characterization techniques

Membrane cross-sections were analyzed with a Hitachi S-4500 scanning electron microscopy (SEM) using a low vacuum and operating at a spatial resolution of 1.5 nm. Membrane cross-sections were obtained by freeze-fracturing the dried membranes in liquid nitrogen. The crystal structures of the samples under study were analyzed by powder X-ray diffraction (XRD) on a Bruker D2 PHASER operated at 40 mA and 40 kV using CuKα radiation with a wavelength (λ) = 1.54 Å. Scans were made from 5° to 50° 2θ with a step size of 0.02° and a scan speed of 0.2 s per step. Thermal stability of the membranes was investigated by thermogravimetric analysis (TGA) using a PerkinElmer TGA-4000. Samples were heated in N_2 from 50 °C to 900 °C at a ramp of 20 °C/min. The values reported in this study are an average of 3 membranes. The glass transition temperature (Tg) of the membranes was determined on a PerkinElmer 8000 differential scanning calorimeter. The samples were heated to a temperature of 400 °C at a temperature ramp of 10 °C/min. Then, the samples were quenched back to 50 °C at 10 °C/min. This cycle was repeated twice and Tg was determined from the second cycle. ^{1}H NMR (Nuclear Magnetic Resonance) spectra were recorded on a 300-MHz Bruker ACF300 spectrometer using deuterated chloroform as solvent (chloroform-d, Sigma-Aldrich, 99.9%). The mechanical properties of prepared MMMs were investigated by utilizing dynamic mechanical analyzer (DMA-Q800) at a frequency of 2 Hz. Dense flat sheet membrane samples with approximate dimensions of 17 × 5 × 0.1 nm were

mounted in the jaws. Each measurement was repeated 3 times and showed a typical standard deviation of ±0.3 GPa for Young's modulus and ±1 MPa for tensile strength. Fourier transform infrared spectroscopy (FTIR) was performed on a FTIR 710 over the wavelength range of 400–4000 cm^{-1}, with a spectral resolution of 4 cm^{-1} and 32 scans. N_2 physisorption measurements were performed on a Tristar 3000 (Micromeritics) and a Quantasorb Autosorb AS-1 (Quantachrome Instruments) at 77 K. Argon physisorption measurements were also performed on a Quantasorb Autosorb AS-1 at 87 K and 77 K. Before measurement, samples were degassed overnight at 150 °C.

Mercury intrusion porosimetry (MIP) measurements were performed with 2 Thermo-Finnigan instruments, Pascal 140 for the range 4–100 μm diameter, and Porosimeter 2000 for the range 0.008–15 μm diameter. Measurement starts at vacuum up to 2 bars, followed by measurement from 1 to 2000 bar. Samples were pre-activated as mentioned before, then quickly transferred to the dilatometers, closed and a vacuum pulled until less than 1 mbar for 1 h. Calculations were performed using a contact angle 140° and surface tension of 480 Dyne cm^{-1}. For particle size calculations, the Mayer and Stowe method was used to calculate particle size, assuming spherical particles [41].

Gas sorption measurements of prepared membranes and pure H-ZIF-8 were performed on a Rubotherm Prazisions Messtechniek magnetic suspension balance, as explained elsewhere [24]. A weighed sample was evacuated till constant weight was achieved. The pressure was then increased by introducing either pure CO_2 or pure CH_4 into the system. The measurement was conducted at different pressures up to 15 bar. The temperature was kept constant at 35.0 ± 0.5 °C.
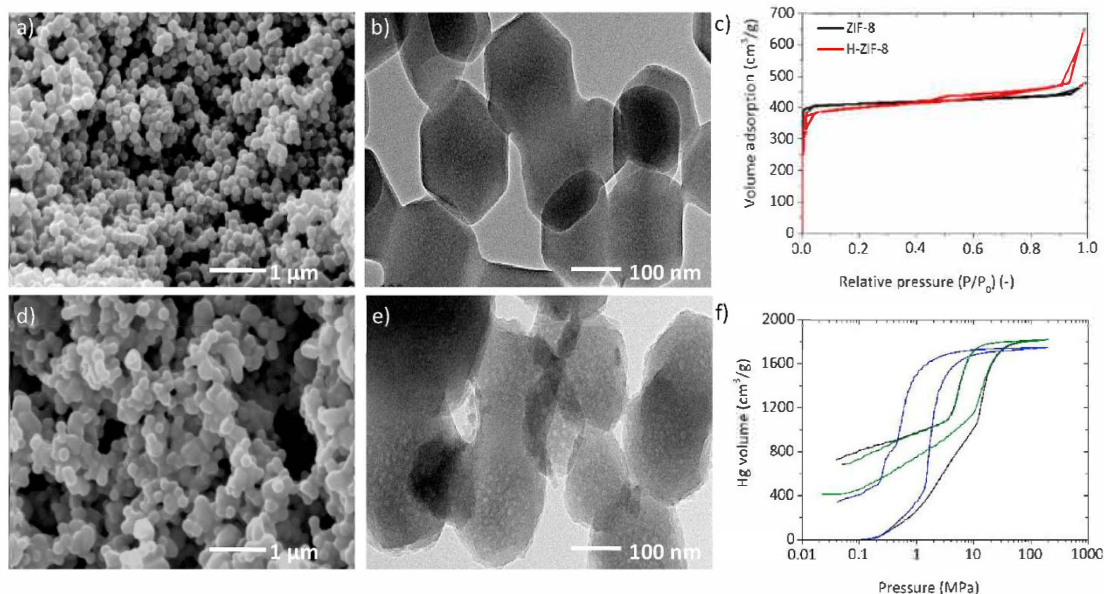
Fig. 2. Characterization of ZIF-8 and H-ZIF-8 materials by (a, d) SEM and (b, d) TEM images and (c) N_2 physisorption: ZIF-8 (black), H-ZIF-8 (red) and (f) Hg intrusion/extrusion measurements: ZIF-8 (blue), H-ZIF-8 first (black) and second (green) intrusion/extrusion. a, b: ZIF-8 and d, e: H-ZIF-8. (For interpretation of the references to colour in this figure legend, the reader is referred to the Web version of this article.)

2.7. Gas separation experiments

Gas permeability measurements were performed using a constant volume permeation cell with vacuum at the permeate side, as described elsewhere [42]. The desired feed pressure was applied at the top side of the membrane while keeping the permeate side under vacuum. The gas permeability values were calculated based on pressure increment (dp/dt) at steady state, according to equations (S4) and (S5). Binary (CO_2/CH_4) gas mixtures with different compositions were used to investigate the membrane performance. All membranes were vacuum heated overnight prior to testing. In every gas separation experiment, two samples from different membranes of the same composition were measured. To exclude time effects, permeability values were taken after 4 h of measurement. During permeation, the composition of feed and permeate were analyzed continuously by a Varian 3900 GC gas chromatograph using an Alltech alumina F-1 60/80 packed bed column. The gas selectivity (α) was calculated by the following relationship:

$$\alpha_{i/j} = \frac{y_i/y_j}{x_i/x_j} \tag{1}$$

Where y_i and y_j are the mole fractions of the components in permeate, while x_i and x_j are their corresponding mole fractions in the feed. The permeability and selectivity values reported are the average of 2–3 membranes. All obtained data have been repeated with an average of deviation of ±10%.

3. Results and discussion

3.1. Preparation and characterization of H-ZIF-8

Various approaches have been reported to prepare mesoporous MOFs, via ligand extension, soft templating, microemulsion or nanocrystal self-assembly [43–45]. The use of extended linkers is an attractive approach to prepare mesoporous MOFs.

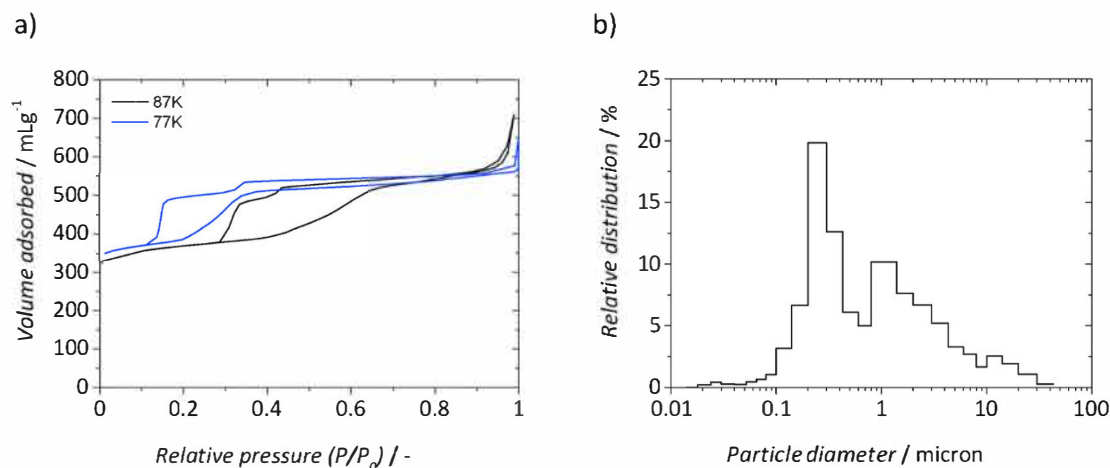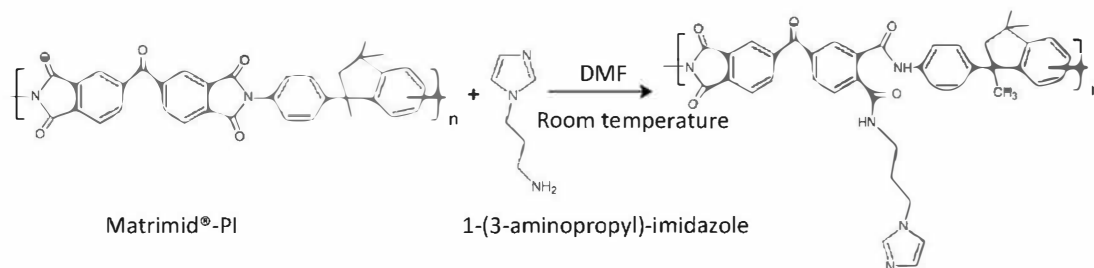However, in most cases, the obtained structure tends to catenate

Fig. 3. (a) Ar isotherms of H-ZIF-8 at 87 K (black) and 77 K (blue); (b) article size analysis of H-ZIF-8 first Hg intrusion measurement. (For interpretation of the references to colour in this figure legend, the reader is referred to the Web version of this article.)

Scheme 1. Grafting of 1-(3-aminopropyl)-imidazole on Matrimid®.

upon the removal of guest molecules during the activation process [45]. Herein, a simple yet highly reproducible method for the preparation of H-ZIF-8 material with excellent surface area and pore volume is presented. Microporous ZIF-8 was locally transformed to a permanent H-ZIF-8 structure by post-synthesis thermal treatment with oleic acid in tert-butanol. Phase purity of ZIF-8 and H-ZIF-8 was confirmed by XRD (Fig. 1). Virtually identical XRD patterns were observed for ZIF-8 and H-ZIF-8. The comparison between the as-synthesized ZIF-8 and the previously reported XRD pattern of ZIF-8 matched well [26], indicating that the ZIF-8 structure was preserved after acid leaching.
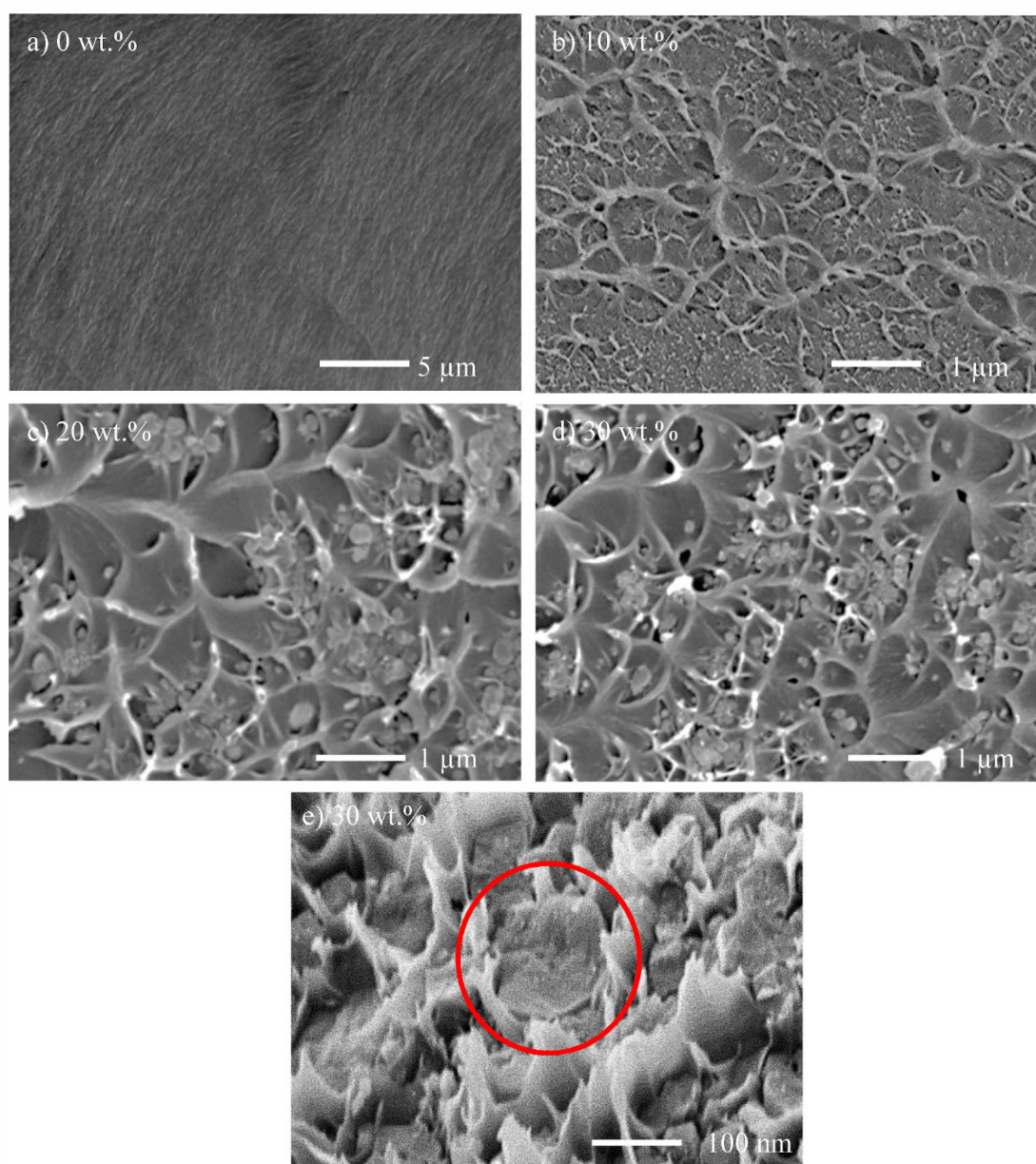

Fig. 4. SEM images of (a–d) the MMM containing 0 to 30 wt% of H-ZIF-8, (e) magnified image of 30 wt% H-ZIF-8 MMM. The red circle surrounds a ZIF-8 particle. (For interpretation of the references to colour in this figure legend, the reader is referred to the Web version of this article.)

Fig. 2a, d shows SEM images of the as-synthesized ZIF-8 and H-ZIF-8 particles, respectively. The average crystal dimension was ca. 150 nm for both ZIF particles. The H-ZIF-8 crystals appear as spheres according to SEM imaging in comparison to the much better defined ZIF-8 crystals (Fig. 2a). The observed rounding effect is probably due to the etching of edges of the nanocrystals. Leaching of Zn from the local structure of ZIF-8 led to the development of internal cavities with defect sites, as evident by in situ FTIR studies using CO as probe molecule [40]. TEM imaging (Fig. 2b, e) of the H-ZIF-8 sample indeed showed the formation of mesostructures inside the ZIF-8 crystals having an average pore diameter of ca. 5–10 nm. This new mesopore feature of H-ZIF-8 was further confirmed by N_2 physisorption analysis which reveals a distinctive Type H2 hysteresis loop coexisting with its original Type I isotherm, (Fig. 2c and Fig. S1), confirming the presence of both micro- and mesopores. Table S1 summarizes the physicochemical properties of both ZIF-8 and H-ZIF-8.

The hysteresis indicates the presence of mesoporosity in the H-ZIF-8 material, and the drop around P/P_0 around 0.45 in the desorption branch is due to sudden cavitation of mesopores through narrow necks. In order to further investigate the secondary mesostructured property of H-ZIF-8, Ar isotherm was measured at 87 K (Fig. 3a). Ar measurements for H-ZIF-8 further confirms the cavitation around 0.4 P/P of rather large mesopores only accessible through narrow necks. To further identify these restrictions, a measurement was performed at 77 K following the method of Thommes (Fig. 3a) [46,47]. The isotherm shifts to lower P/P_0 at the lower temperature as expected but keeps the same step size at the cavitation jump, now occurring around $P/P_0 = 0.35$ for 77 K [41]. This not only confirms the cavitation phenomenon through narrow necks, but.

as at 77 K all pores cavitate below 12 nm (upper limit of pore determination at 77 K) this means that most of these mesopores are larger than 4 nm, the lower limit for cavitation at 87 K.

Assuming uniform intra-crystalline cavities of around 10 nm, one should have 60 cavities per 100 nm crystal. The TEM image (Fig. 2e) agrees with this estimation. To further verify the accessibility of the mesoporous cavities in H-ZIF-8, mercury intrusion porosimetry (MIP) was performed as shown in Fig. 2f. With a maximum pressure of 200 MPa, only pores above 8 nm could be probed, and no mercury penetrates the micropores. The microporous ZIF-8 shows a sharp rise at 2 MPa, pointing at "pores" around 1 nm indicating interparticle voids attributed to the formation of crystal agglomerates. The H-ZIF-8 shows a gradual rise followed by a sharper step at 20 MPa, pointing at a broad range of porosity for large pores. The sharper rise corresponds with the crystals in the range of 100–1000 nm centered ca. 200 nm (Fig. 3b), corresponding well with the SEM and TEM images (Fig. 2d and e). More importantly, at pressures above 60 MPa, there is no further penetration and hence there are no accessible pores between 50 and 8 nm (lower limit of the measurement at 200 MPa). This confirms that most of the larger mesoporous cavities seen in TEM, N_2 and Ar measurements are only accessible through narrow necks. Above results are further explained in detail in the supporting information.

The thermal stability of the H-ZIF-8 material, as analyzed by TGA in nitrogen atmosphere shows no significant weight loss till 200 °C (Fig. S2), indicating the hydrophobic characteristic of ZIF-8 [48]. At temperatures above 450 °C, degradation of the H-ZIF-8 structure occurs. A similar behavior of thermal decomposition of ZIF-8 was reported by Basu et al. and Cavillon et al. [49,50]. The preparation of H-ZIF-8 did not cause a significant change in crystal structure as confirmed by XRD and TGA, despite its textural and pore structure alteration.

3.2. Polymer modification via 1-(3-aminopropyl)-imidazole grafting

The grafting of 1-(3-aminopropyl)-imidazole on PI was done via imide ring opening (as shown in Scheme 1). The reaction was carried out in dioxane/DMF (40/60 ratio) under stirring at 25 °C for 3–4 h. PI was modified to a degree of 50% and 100%. The chemical structures of the

Table 1
Properties of MMMs with different H-ZIF-8 loadings.

H-ZIF-8 loading [wt.%]	Tg [°C][a]	Density ρ_M [g/ cm^3]	Young's modulus [GPa]	Tensile strength [MPa]	Elongation at break [%]
0	278	1.20	2.50	105	115
10	282	1.26	2.81	93	102
20	287	1.29	3.32	90	91
30	293	1.33	3.51	80	83

[a] (Typical error in DSC results ranges from ±1–1.5 °C).

resulting materials, referred to as modified Matrimid®-PI (M-PI) from now on, were confirmed by 1H NMR (Figs. S3–S4) and FTIR (Fig. S5). The percentage of modification was evaluated by 1H NMR. Details of the calculation of the modification degree are given in the supporting information. The chemical modification of the polymer chains makes the system more flexible, while amine modification of PI has been reported to result in gas separation membranes with improved gas productivity [51].

3.3. MMM characterization

The characteristics of the H-ZIF-8-MMMs were studied by a multitude of characterization techniques, such as XRD, FTIR, NMR, TGA, DSC, and SEM. Fig. 4 shows the SEM cross-sectional morphology of M-PI and H-ZIF-8 MMMs with different H-ZIF-8 loadings. The unfilled M-PI membrane shows the typical smooth surface morphology without any plastic deformation upon fracture. The overall morphology of the MMMs shows good embedment of the H-ZIF-8 particles within the matrix, indicating a homogeneous distribution.

Fig. 4b–d shows the crater-like morphology, typical for MMMs, in which the crater's eye is formed by a H-ZIF-8 particle. As the H-ZIF-8 loading increases, the size of the craters becomes smaller. A more magnified image of the MMM is shown in Fig. 4e. No obvious agglomeration of H-ZIF-8 particles can be observed. The H-ZIF-8 particles are completely wrapped by a very thin layer of polymer and they are well distributed over the cross section. Fig. 4e shows a good interaction between the H-ZIF-8 particles and the M-PI matrix in more detail, most probably due to improved affinity between MOF and M-PI chains via grafting of imidazolate linkages [24]. As the H-ZIF-8 has a mesoporous structure, the polymer chains in the vicinity of the MOF may penetrate into the pores of the MOF, which can further contribute to enhanced compatibility between the ZIF-8 particles and polymer matrix [52,53].

XRD patterns of the unfilled polymer and the MMMs are presented in Fig. S6. The M-PI membrane is completely amorphous and shows a broad peak, typical of an amorphous structure material. For H-ZIF-8 MMMs, the presence of the H-ZIF-8 phase is confirmed through intense crystalline peaks, clearly similar to those of pure H-ZIF-8. Moreover, the intensity of crystalline peaks of H-ZIF-8 MMMs increases with increasing H-ZIF-8 loading. The thermal stability of M-PI, H-ZIF-8 and M-PI/H-ZIF-8 MMMs is presented in Fig. S7. H-ZIF-8 shows a degradation temperature of 450 °C, in agreement with literature [49]. The M-PI/H-ZIF-8 MMMs exhibit two stages of significant weight loss: first in the range of 150 °C–300 °C, due to the removal of moisture and trapped residual solvent, second from 450 °C onwards, due to the decomposition of M-PI matrix and H-ZIF-8.

The Tg and mechanical properties of MMMs are presented in Table 1. The Tg of unfilled Matrimid® is 328 °C, consistent with reported data [54]. The surface modified unfilled M-PI membrane shows a Tg around 278 °C. This drop in Tg can be attributed to the plasticization effect caused by the 1-(3-aminopropyl)-imidazole surface modifier (as GPC molecular weight measurement showed no reduction in molecular weight). The Tg values of the MMMs are slightly higher than those of the unfilled M-PI membrane, increasing up to 293 °C for the 30 wt% H-ZIF-8 MMM.

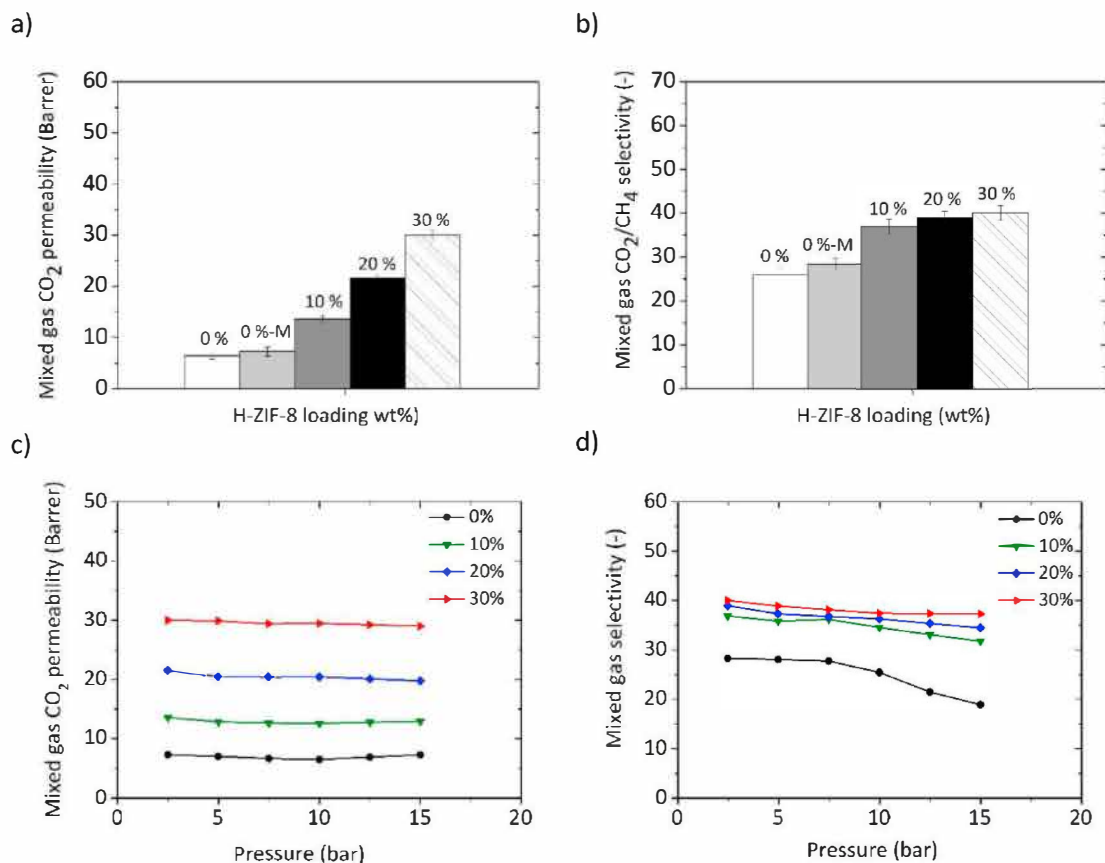Introduction of H-ZIF-8 in the polymer matrix causes the formation

Fig. 5. Mixed gas (CO_2/CH_4 50/50 vol %) a) CO_2 permeability, b) CO2/CH$_4$ selectivity of H-ZIF-8 MMMs at 2.5 bar and 35 °C; c) CO_2 permeability and d) CO_2/CH_4 selectivity of MMMs as a function of feed pressure.

of physical crosslinks between the polymer chains and the MOF particles. Moreover, the hierarchical pore structure of H-ZIF-8 allows the penetration of polymer chains into the MOF surface. This creates extra entanglements and changes the polymer-particle interactions and the relative orientation of the chains, leading to a more rigid intermediate phase with relatively higher Tg. The incorporation of H-ZIF-8 particles in the M-PI matrix up to 30 wt% loading results in a linear increase in Young's modulus, while elongation at break (%) and tensile strength decrease. The improved mechanical properties can be reasoned to enhance interfacial adhesion between the H-ZIF-8 particles and polymer chains, as attributed to the interaction between the imidazolate moiety of M-PI and H-ZIF-8 [24].

3.4. Gas separation

3.4.1. Effect of H-ZIF-8 loading and CO_2 feed pressure

Due to the CO_2 sorption of the polymer matrix and the associated locally enhanced polymer mobility, the permeability of the slower component (e.g. N_2 or CH_4) mostly increases to a larger extent than that of CO_2, leading to decreasing (diffusion) selectivity. The results of mixed gas transport data of unfilled M-PI membrane and MMMs with various loadings of H-ZIF-8 are presented in Fig. 5a and b. The unfilled M-PI membrane shows a higher CO_2 permeability compared to that of un-modified PI, as attributed to the interaction between CO_2 and the imi-dazolate moiety of the M-PI chains. Thus, modification of PI membrane not only helps to improve compatibility between H-ZIF-8 and polymer but also contributes positively to the increment of CO_2 permeability. For MMMs with 10 wt%, 20 wt% and 30 wt% H-ZIF-8 loadings, CO_2 permeability increases to 86%, 194%, and 310%, respectively, as compared to unfilled M-PI membrane. It is important to note that CO_2/CH_4 selectivity also increased with increasing H-ZIF-8 loading, which is

not often found in MMM experiments, due to interfacial void creation. The combined improved CO_2 permeability and CO_2/CH_4 selectivity observed for MMMs loaded with H-ZIF-8 can be attributed to (i) the increased free volume [16] in the membrane achieved via the incorporation of H-ZIF-8 particles, (ii) the enhanced compatibility between polymer and H-ZIF-8 particles, and (iii) stronger quadrupole interaction of CO_2 with the grafted imidazolate moieties on the polymer surface as well in H-ZIF-8 [55].

The influence of feed pressure on the membrane performance of the binary gas mixtures was also studied (Fig. 5c and d). The M-PI membrane shows a slight decrease in permeability with an increase in pressure. This decrease in permeability at higher pressures stems from the decreasing solubility (saturation of polymer by gas molecules) with increasing pressure, following the predicted behavior of the dual-mode sorption model equation (S1) [56,57]. As the CO_2 pressure increases further, the M-PI membrane shows an increment in CO_2 permeability due to plasticization by condensable CO_2 above 10 bar, consistent with literature [58–60]. The enhanced chain mobility implies an increase in gas diffusion [60].

All MMMs show a similar trend of decreasing CO_2 permeability with pressure, like that of the unfilled M-PI membrane. However, in contrast to unfilled M-PI membrane, H-ZIF-8 MMMs show no obvious signs of plasticization up to 15 bar (Fig. 5c and Fig. S10). It can be attributed to rigidity introduced by the MOF particles that tend to restrict the polymer chains mobility in MMMs, suppressing polymer network dilation (plas-ticization) [23,42,61]. This restricted mobility, in this case, can be ascribed to the interactions of the polymer with the filler outer surface or to a certain sorption of the polymer chains inside the enlarged pores of the H-ZIF-8. The extent of plasticization suppression is dependent on the introduction of strong ZIF-8/PI interactions, especially at high H-ZIF-8 loading (30 wt%), forming a sturdier and mechanically rigid structure
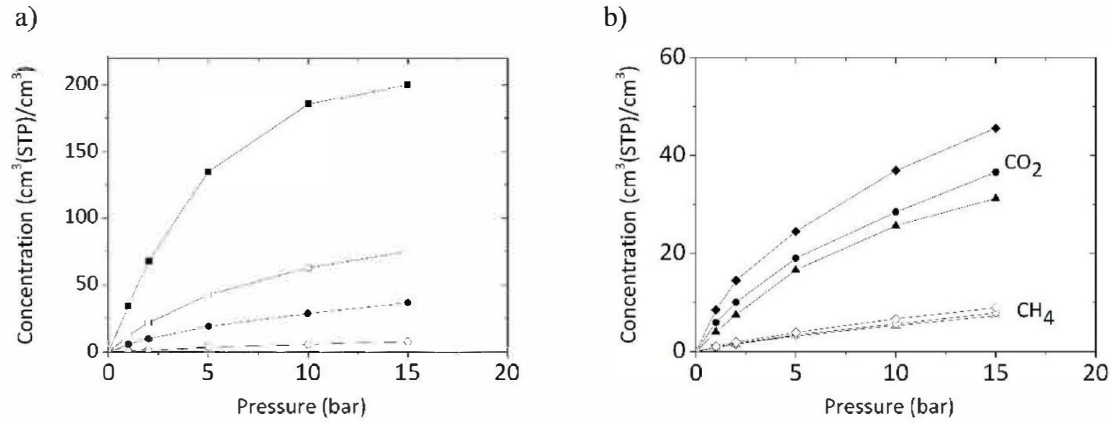
Fig. 6. Sorption isotherms of CO2 (closed) and CH4 (open) of pure ZIF-8 (■, □), pure modified Matrimid® (●, ○), Matrimid® (▲, △) and 20 wt.% H-ZIF-8 MMMs (◆, ◇) as function of the applied gas pressure at 35 °C.

Table 2
Fitted dual-mode sorption and Sips model parameters in the different membranes for CO_2 and CH_4 isotherms.

Gas	H-ZIF-8	Dual mode sorption model			Sips model		
	[wt.%]	C'_H [cm³(STP) cm⁻³]	b [cmHg]	k_D [cm³(STP) cm⁻³ cmHg⁻¹]	C'_s [cm³(STP) cm⁻³]	b_s [cmHg⁻¹]	n (−)
CO₂	0	28.02	0.17	0.75	–	–	–
	0-*M*-PI[a]	35.11	0.18	0.79	–	–	–
	20	50	0.19	0.44	61	0.074	0.86
	100	260	0.24	0	300	0.15	0.94
CH₄	0	10.40	0.054	0.17	–	–	–
	0-*M*-PI[a]	11.51	0.056	0.18	–	–	–
	20	14.50	0.061	0.12	20	0.055	0.80
	100	124.0	0.104	0	140	0.08	0.86

[a] (0-*M*-PI modified Matrimid®).

(Table 1). For all MMMs, a gradual decrease in CO_2/CH_4 selectivity is observed with increasing pressure. However, MMMs show higher CO_2/CH_4 selectivities than the unfilled M-PI membrane over the whole pressure range and CO_2/CH_4 selectivity increases dramatically with increasing H-ZIF-8 loading.

3.4.2. Gas sorption

The sorption capacity of polymer membranes can be increased by incorporating MOFs with a higher sorption capacity into the polymer phase. Therefore, the sorption behavior of CO_2 and CH_4 in the different membranes was investigated (Fig. 6). The sorption isotherms are fitted with both the dual-mode sorption equation (S1) and the Sips model equation (S3) separately, where it is assumed that the MMMs are comprised of one homogeneous phase. The obtained fitting parameters from both models are summarized in Table 2.

CO_2 shows higher sorption compared to CH_4 in all cases, attributed to the higher critical temperature (T_c) and consequently enhanced condensability of CO_2 compared to CH_4 (T_c-CO_2: 304K, T_c-CH_4: 190K) [1]. Also, the favorable quadrupolar interactions of CO_2 with the electron donor groups in the polymer and the MOF contribute to this. M-PI shows a relatively higher CO_2 sorption compared to unmodified PI. Pure H-ZIF-8 shows much higher adsorption attributed to the high surface area (1660 m²/g) of the particles. Addition of 20 wt% H-ZIF-8 leads to an increase in sorption capacity of both gases compared to the unfilled polymer membrane.

The dual-mode sorption parameters for different membranes are compared in Table 2. The higher values of C'_H and b for the MMMs reflect the contribution of H-ZIF-8 in increasing the sorption capacity and sorption affinity of the unfilled M-PI membrane. C'_H is also a measure of the amount of the excess free volume in the polymer thus, the addition of the H-ZIF-8 particles to the polymer matrix could increase the excess free volume of the polymer, which contributes as well to the higher gas sorption [26,62]. In addition, the increase in b indicates that the H-ZIF-8 MMMs show a stronger interaction with the gases compared to the unfilled M-PI membrane. The results tabulated in Table 2 for the MMMs suggest that the addition of H-ZIF-8 in the M-PI membrane affects both the Langmuir and Henry's sorption (dual mode sorption). The high values of Henry's law constants for the unfilled M-PI membrane, compared to MMMs, revealed that the major contribution to the overall sorption in the unfilled M-PI membrane is through the Henry's law sorption. The value of the Henry's law constant (k_D) decreases with increasing H-ZIF-8 loading from 0.79 to 0.44 and 0.18 to 0.12 for CO_2 and CH_4, respectively. This implies that the overall sorption is dominated by Langmuir sorption at higher loadings of H-ZIF-8, as observed for microporous ZIF-8 [24]. The effects of H-ZIF-8 loading on the CO_2 and CH_4 solubility in H-ZIF-8 MMMs are shown in Fig. S9. Sips model parameters show multi-layer sorption in 20 wt% H-ZIF-8 MMM and pure H-ZIF-8. However, the maximum Sips sorption capacity, C'_s, in 20 wt% H-ZIF-8 MMM is decreased by a factor of 5 and 7 for CO_2 and CH_4, respectively, compared to the C'_s in the pure H-ZIF-8. This reduction in Sips sorption capacity of 20 wt% H-ZIF-8 MMM can be explained by sorption limitations of the surrounding polymer layer wrapping the H-ZIF-8 particles.

The gas sorption and separation data are further analyzed using the solution-diffusion model. Fig. 7 presents the measured normalized solubility and diffusion coefficients of CO_2 and CH_4 as a function of H-ZIF-8 loading at 2.5 bar and 35 °C. It is important to note that gas diffusivity was calculated based on pure gas solubility and mixed gas permeabilities
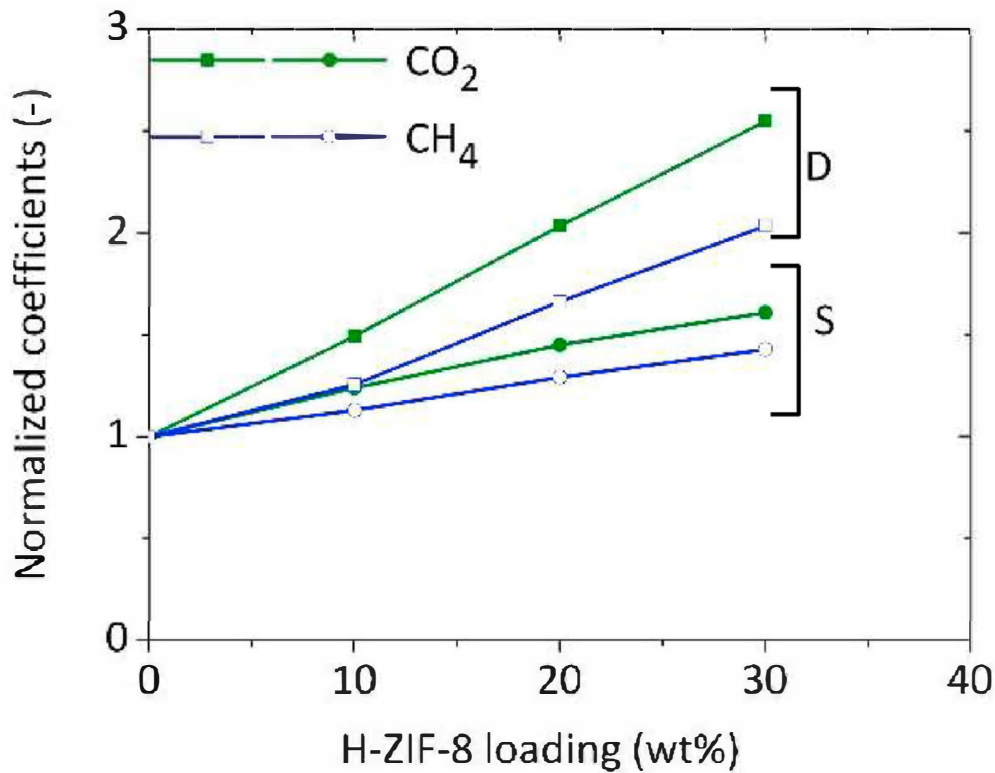
Fig. 7. Normalized solubility (S) and diffusion (D) coefficients for CO_2 (closed symbols) and CH_4 (open symbols) as a function of H-ZIF-8 loading at 2.5 bar and 35 °C.
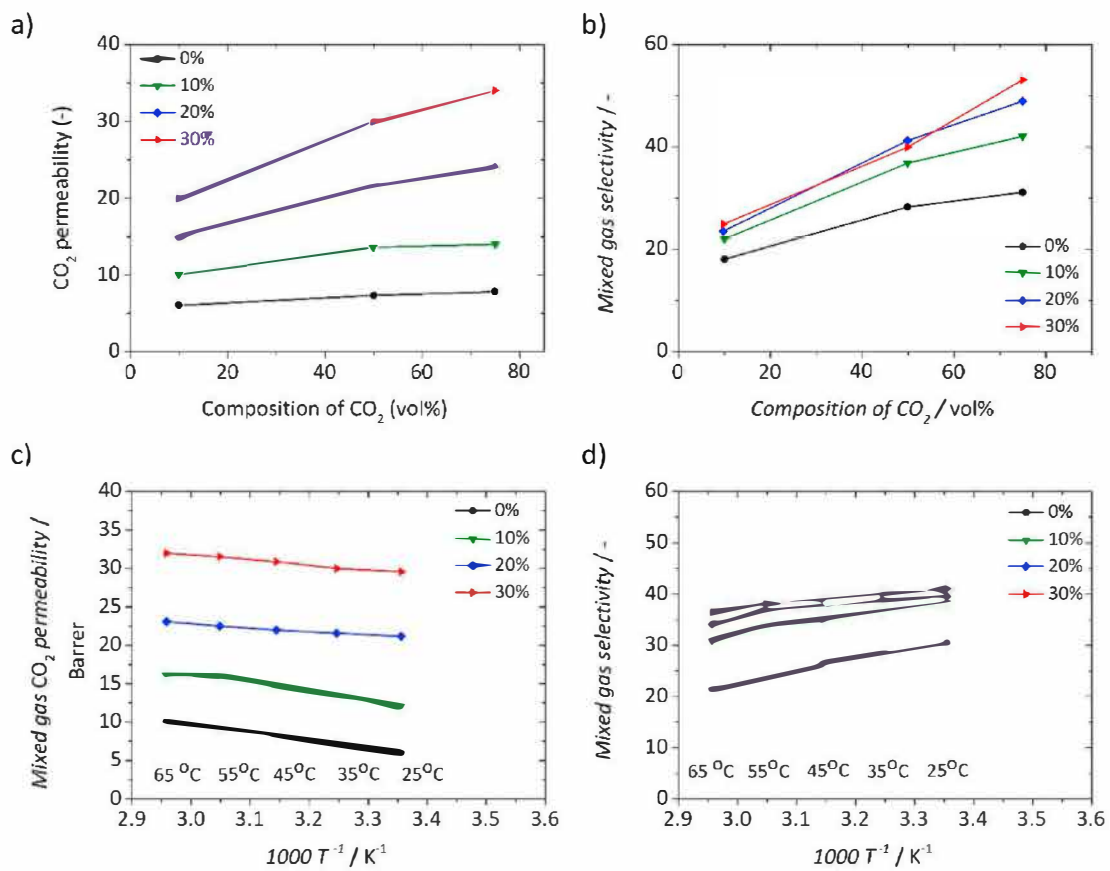

Fig. 8. Mixed gas (a) CO_2 permeability and (b) CO_2/CH_4 selectivity of H-ZIF-8 MMMs as a function of CO_2 composition (vol%) in the binary feed mixture at 2.5 bar and 35 °C. Mixed gas (CO_2/CH_4 50/50 vol%) (c) CO_2 permeability and (d) CO_2/CH_4 selectivity of H-ZIF-8 MMMs as a function of temperature at 2.5 bar.
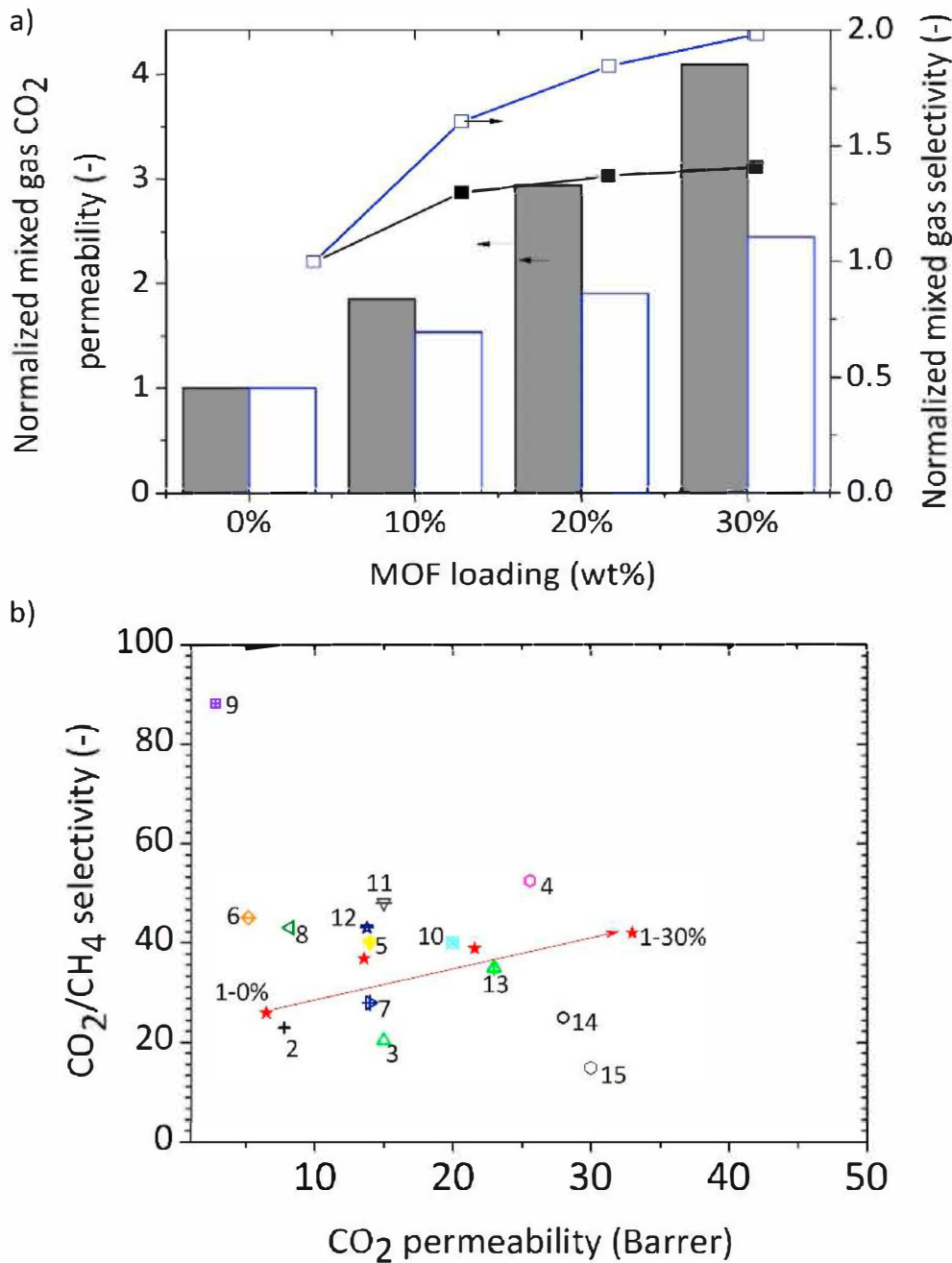
a)

b)

Fig. 9. (a) Comparison of microporous ZIF-8 MMMs (blue open bars and symbols) and H-ZIF-8 MMMs (black close bars and symbols) at 2.5 bar and 35 °C, (b) Comparison of CO_2/CH_4 mixed gas separation performance of H-ZIF-8 containing Matrinid® MMMs (this work-red closed star symbols) with different MOF fillers. See Table 3 for details of different membranes and experimental details. (For interpretation of the references to colour in this figure legend, the reader is referred to the Web version of this article.)

($D = P_{mix}/S_{pure\ gas}$), thus the estimated values of D only provides a general trend of diffusivity of gases with H-ZIF-8 loading. As the mixed gas permeability is known to be slightly lower than the pure gas permeabilities due to competitive sorption the diffusivity values in Fig. 7 should slightly underestimated than the actual diffusivity values. The data were normalized based on the data of unfilled M-PI membrane. The normalized CO_2 diffusivity increases more than the normalized diffusivity of CH_4 up to 30 wt%, but the normalized solubility of CO_2 is comparable to that of CH_4. Therefore, permeability differences are mainly determined by their CO_2 diffusivities. Since H-ZIF-8 has a mesoporous structure, it could reduce the transport resistance in MMMs and enhances the CO_2 diffusivity. It has been reported that the self-diffusion coefficient of gas in the hierarchical MOFs is much faster than in the microporous MOF [63]. According to the literature, CO_2 experiences a lower energy barrier for diffusion than for CH_4 in microporous ZIF-8, and therefore a higher CO_2 diffusivity is achieved [64]. Similar gas

sorption behavior could also be speculated in H-ZIF-8, despite further experimental and simulation works are needed to confirm this hypothesis.

In addition to CO_2 permeability enhancement, the incorporation of H-ZIF-8 also leads to a moderate increase in the mixed gas CO_2/CH_4 selectivity. When the MOF loading increases, it is noted that CO_2 is more permeable than CH_4, which consequently increased the CO_2/CH_4 selectivity of the MMMs. It is important to note that the normalized solubility coefficients (solubility selectivity) for CO_2 and CH_4 cannot solely be taken into account for this increase in CO_2/CH_4 selectivity. Therefore, the increase in CO_2/CH_4 selectivity can be majorly attributed to the moderate increase in diffusivity of CO_2 over CH_4. These results also suggest that the mesoporous cavities in H-ZIF-8 are only accessible by the microporous pores via smaller apertures, in good agreement with the N_2, Ar and MIP results. These narrow necks can effectively limit the size of molecules that can diffuse into the functional void space, thus

Table 3
Performance of composite membranes with different fillers (data presented in Fig. 9b).

MOF[a]	Polymer[a]	Wt% loading	Examples (best performance)			Type of analysis	Operational conditions		Reference
			P_{CO_2} [Barre]	CO_2/CH_4 Selectivity (−)	Graph code[b]		T [°C]	ΔP [bar]	
H-ZIF-8	Matrimid®	0–30	30	39.95	1	Mixed gas 50:50	35	5	This work
FeBTC	Matrimid®	–	7.8	23	2	Mixed gas 50:50	35	2	[42]
Cu-BPY-HFS	Matrimid®	20		20.5	3	Mixed gas 50:50	35	2	[17]
ZIF-8	Matrimid®	30	25.61	52.4	4	Mixed gas 50:50	35	5	[24]
ZIF-8-ambz	Matrimid®	15	14	40	5	Mixed gas 50:50	35	3.5	[22]
NH2-MIL-53(Al)	Matrimid®	20	8.2	43	6	Mixed gas 50:50	35	3	[69]
UiO-66NH₂	Matrimid®	30	14	28	7	Mixed gas 50:50	35	3	[20]
B-CuBDC	Matrimid®	8	5.2	45	8	Mixed gas 50:50	25	3	[70]
NS-CuBDC	Matrimid®	8	2.8	88.2	9	Mixed gas 50:50	25	3	[70]
ZIF-8	Matrimid®/PSF	30	20	40	10	Mixed gas 50:50			[61]
CuBTC	Matrimid®	30	15	48	11	Mixed gas 50:50	35	5	[23]
Sod-ZMOF	Matrimid®	20	13.79	43	12	Mixed gas 50:50	35	0.4	[71]
ZIF-8	Matrimid®	20	22	35	13	Mixed gas 50:50	35	4	[66]
ZIF-8	Matrimid®	30	28	25	14	Mixed gas 50:50	22	4	[26]
ZIF-8	Matrimid®-PEG(4%)	30	30	15	15	Mixed gas 50:50	25	8	[27]

[a](Abbreviation: 6FDA: 4,4-(hexa fluoro isopropylidene) diphthalican hydride; Durene: 2,3,5,6-tetramethyl- 1,4-henylenediamine; ODA: 4,4′ 6oxydianiline; IRMOF-1: Zn4O(1,4-benzene-dicarboxylate)₃; Cu-BPY-HFS: copper hexa fluorosilicate (HFS) and 4,4′-bipyridine (BPY); NH2-MIL-53(Al): amino-aluminum terephthalate; ambz: 2-amino-benzimidazole; UiO-66(Zr-BPDC): (BPDC¼biphenyl- 4,4′-dicarboxylate), ZIF-8: zeolite imidazolate framework-8, ZIF-90: zeolite imidazolate framework-90; NH₂-MOF-199 (CuBTC): Cu-benzene-1,3,5-tricarboxylate (BTC); P1: all-aromatic diamine (1,4-bis(4 aminophenoxy) benzene; DAM: 2,4,6-trimethyl-*m*-phenyl-enediamine; BDC: 1,4-benzenedicarboxylate NS: nanosheets; B: bulk; FeBTC: Fe-benzene-1,3,5-tricarboxylate; Ultem: polyetherimide; PSF: polysulfone); [b](Code of different publications represented in Fig. 6b).

also providing a moderate diffusion selectivity.

3.4.3. Effect of feed composition and operating temperature

The gas separation performances of unfilled M-PI membrane and H-ZIF-8 MMMs were measured for three different CO_2/CH_4 gas compositions. Fig. 8a shows the normalized CO_2 permeability as a function of CO_2 concentration (%) in the mixed feed. Normalization is done by dividing all permeabilities by the initial permeability at 10% CO_2 gas in the feed mixture. CO_2 permeability for all membranes increases with increasing CO_2 concentration in the feed mixture. As the loading of H-ZIF-8 increases, the results show a swifter increase in CO_2 permeability. At very low CO_2 concentration, CO_2 and CH_4 adsorb in a non-competitive way inside the pores of H-ZIF-8. With increasing pressure, the pores become gradually filled and competitive adsorption favors the adsorption of CO_2 over CH_4. With increasing CO_2 loading in the H-ZIF-8 pores, the intrapore diffusion constant increases, resulting in an increase in the mixed gas CO_2 permeability and CO_2/CH_4 the selectivity increases as a function of CO_2 concentration in the feed (Fig. 8b and Fig. S11).

The effect of temperature on binary gas mixture selectivity and CO_2 permeability is presented in Fig. 8c and d as a function of inverse absolute temperature. The CO_2/CH_4 selectivity shows a decrease with increasing temperature (higher temperatures increase the gas permeability), similar to Yuan and co-workers [65]. For the M-PI membrane, CO_2 permeability increased by 63% while declining CO_2/CH_4 selectivity by 29% when temperature increases to 65 °C. On the contrary, H-ZIF-8 MMMs show a relatively lower decrease in selectivity over the entire temperature ranges tested, as attributed to the rigidity introduced by the H-ZIF-8 particles in the MMMs (Table 1) [66]. Fig. 8c shows a typical Arrhenius relation and the increase of permeability with temperature and can be well described by equation (S8).

The gas flux of all penetrants increases with increasing temperature (Fig. 8c and Fig. S12) due to increased mobility and flexibility of the polymer chains and higher kinetic energies of the permeating molecules. Temperature increases enhance the permeability of both gases, while selectivity decreases. In general, the positive effect of temperature on gas transport and sorption behavior is more significant than the negative effect of temperature on solubility [24].

The activation energy of permeation (Ep) is calculated from equation (S8) and given in Table S2. It can be readily seen that the incorporation of H-ZIF-8 in the MMMs decreases the Ep-values of CO_2 and CH_4 as compared to the unfilled M-PI membrane. This result confirms that a significant increase in gas diffusivities is achieved upon the incorporation of H-ZIF-8. Lower Ep values suggest that smaller molecules like CO_2 can execute diffusive jumps through the transient chain gaps in the polymeric chains, as larger molecules, like CH_4, would experience greater diffusional resistance [67].

3.4.4. Comparison of ZIF-8 and H-ZIF-8 MMMs versus other reported MMMs for CO_2/CH_4 separation

Fig. 9a shows the comparison of MMMs containing ZIF-8 and H-ZIF-8. The permeability of CO_2 increases for both MMM systems as the MOF loading increases. However, it should be noted that the H-ZIF-8 loaded MMMs show a more significant increase in gas permeability with increasing H-ZIF-8 loading than the ZIF-8 MMMs. The results indicate the importance of a mesopore structure present in H-ZIF-8 to allow a faster transport of gases. A less pronounced difference in CO_2/CH_4 selectivity is observed for H-ZIF-8 loaded MMMs as compared to the ZIF-8 MMMs due to the slightly higher permeability of CH_4 through H-ZIF-8 MMMs (Fig. S13) [63]. In addition, the enhanced performance of H-ZIF-8 MMMs can also be related to the presence of defects (missing metal coordination sites) inside the H-ZIF-8 structure, which can lead to increased CO_2-metal interactions [68]. The performances of fabricated M-PI/H-ZIF-8 composite membranes were compared with those of polyimide based composite membranes introducing different fillers (Fig. 9b and Table 3). M-PI/H-ZIF-8 membrane showed a high CO_2 permeability of 30 Barrer with CO_2/CH_4 selectivity of 40 at the feed gas pressure of 2.5 bar and 35 °C. Addition of H-ZIF-8 enhances the performance for CO_2/CH_4 separation, mainly resulted from the good polymer-MOF interfacial compatibility, porosity of H-ZIF-8 nanoparticles. M-PI/H--ZIF-8-30 wt% membrane marks a promising selectivity/permeability combination with highest ever reported CO_2 permeability, especially when the performance of MMMs was investigated with binary gas mixtures CO_2/CH_4 under a variety of operating conditions using cheap, commercially available polymers, like Matrimid®. These results

highlight the importance of MOF fillers with interconnected hierarchical structures for improving the membrane molecular separation of CO_2/CH_4 performance by enhancing the sorption and diffusion inside these hierarchical MOF crystals embedded in the polymer matrix.

4. Conclusions

The molecular separation performance of CO_2 over CO_2/CH_4 binary mixtures was enhanced via MMMs with incorporated submicron-sized hierarchical ZIF-8 molecular sieves. This study revealed that the incorporation of hierarchical ZIF-8 filler into the polymer matrix creates additional free volume and interaction sites to simultaneously boost the permeability and selectivity of the H-ZIF-8 MMMs as compared to microporous ZIF-8 loaded MMMs or unfilled Matrimid® membranes. Gas sorption studies further confirmed that the selective gas transport is mainly governed by an increase in diffusion selectivity, which is always higher than the solubility selectivity of H-ZIF-8 MMMs. No plasticization was observed for the MMM containing 30 wt% H-ZIF-8 particles up to 15 bar CO_2 partial pressure, while the M-PI membrane plasticizes at about 10 bar CO_2 partial pressure. The improved plasticization resistance was attributed to chain mobility restrictions, resulting from the interactions between H-ZIF-8 and M-PI. The introduction of hierarchical MOFs with specific arrangement of mesostructures interconnected through narrow neck pores in the interior of microporous ZIF-8 particles thus allows a better control over their gas transport properties, leading to MMMs with highly improved CO_2 permeability, the presented strategy offering the combined synergistic effects of membrane stability and performance improvement should be generally applicable to many other challenging gas separations, such as hydrocarbons and olefin/paraffin separations.

Author statement

The manuscript was written through contributions of all authors. All authors have given approval to the final version of the manuscript. Author S. Shahid is the main writer, investigator and data generator of the manuscript. Other authors contributed in data generation, validation, reviewing and editing.

Declaration of competing interest

The authors declare that they have no known competing financial interests or personal relationships that could have appeared to influence the work reported in this paper.

Acknowledgments

Appendix A. Supplementary data

Supplementary data to this article can be found online at https://doi.org/10.1016/j.memsci.2020.118943.

References

[1] N.N. Li, A.G. Fane, W.S.W. Ho, T. Matsuura, Advanced Membrane Technology and Applications, 2008.

[2] R.W. Baker, Future directions of membrane gas separation technology, Ind. Eng. Chem. Res. 41 (2002) 1393–1411.

[3] S. Basu, A.L. Khan, A. Cano-Odena, C. Liu, I.F.J. Vankelecom, Membrane-based technologies for biogas separations, Chem. Soc. Rev. 39 (2010) 750–768.

[4] P. Bernardo, E. Drioli, G. Golemme, Membrane gas separation: a review/state of the art, Ind. Eng. Chem. Res. 48 (2009) 4638–4663.

[5] Y. Xiao, B.T. Low, S.S. Hosseini, T.S. Chung, D.R. Paul, The strategies of molecular architecture and modification of polyimide-based membranes for CO2 removal from natural gas—a review, Prog. Polym. Sci. 34 (2009) 561–580.

[6] M. Hegde, S. Shahid, B. Norder, T.J. Dingemans, K. Nijmeijer, Gas transport in metal organic framework-polyetherimide mixed matrix membranes: the role of the polyetherimide backbone structure, Polymer 81 (2015) 87–98.

[7] L.M. Robeson, Correlation of separation factor versus permeability for polymeric membranes, J. Membr. Sci. 62 (1991) 165–185.

[8] L.M. Robeson, The upper bound revisited, J. Membr. Sci. 320 (2008) 390–400.

[9] J.T. Chen, C.C. Shih, Y.J. Fu, S.H. Huang, C.C. Hu, K.R. Lee, J.Y. Lai, Zeolite-filled porous mixed matrix membranes for air separation, Ind. Eng. Chem. Res. 53 (2014) 2781–2789.

[10] D.Q. Vu, W.J. Koros, S.J. Miller, Mixed matrix membranes using carbon molecular sieves - I. Preparation and experimental results, J. Membr. Sci. 211 (2003) 311–334.

[11] M. Waqas Anjum, F. de Clippel, J. Didden, A. Laeeq Khan, S. Couck, G.V. Baron, J. F.M. Denayer, B.F. Sels, I.F.J. Vankelecom, Polyimide mixed matrix membranes for CO2 separations using carbon–silica nanocomposite fillers, J. Membr. Sci. 495 (2015) 121–129.

[12] A. Sabetghadam, B. Seoane, D. Keskin, N. Duim, T. Rodenas, S. Shahid, S. Sorribas, C.L. Guillouzer, G. Clet, C. Tellez, M. Daturi, J. Coronas, F. Kapteijn, J. Gascon, Metal organic framework crystals in mixed-matrix membranes: impact of the filler morphology on the gas separation performance, Adv. Funct. Mater. 26 (2016) 3154–3163.

[13] A. Kertik, L.H. Wee, M. Pfannmoller, S. Bals, J.A. Martens, I.F.J. Vankelecom, Highly selective gas separation membrane using in situ amorphised metal-organic frameworks, Energy Environ. Sci. 10 (2017) 2342–2351.

[14] P.S. Goh, A.F. Ismail, S.M. Sanip, B.C. Ng, M. Aziz, Recent advances of inorganic fillers in mixed matrix membrane for gas separation, Separ. Purif. Technol. 81 (2011) 243–264.

[15] H.B.T. Jeazet, C. Staudt, C. Janiak, Metal-organic frameworks in mixed-matrix membranes for gas separation, Dalton Trans. 41 (2012) 14003–14027.

[16] E.V. Perez, K.J. Balkus Jr., J.P. Ferraris, I.H. Musselman, Mixed-matrix membranes containing MOF-5 for gas separations, J. Membr. Sci. 328 (2009) 165–173.

[17] Y. Zhang, I.H. Musselman, J.P. Ferraris, K.J. Balkus Jr., Gas permeability properties of Matrimid (R) membranes containing the metal-organic framework Cu-BPY-HFS, J. Membr. Sci. 313 (2008) 170–181.

[18] S. Basu, A. Cano-Odena, I.F.J. Vankelecom, Asymmetric Matrimid (R)/Cu-3(BTC) (2) mixed-matrix membranes for gas separations, J. Membr. Sci. 362 (2010) 478–487.

[19] R. Thür, N. Van Velthoven, S. Slootmaekers, J. Didden, R. Verbeke, S. Smolders, M. Dickmann, W. Egger, D. De Vos, I.F.J. Vankelecom, Bipyridine-based UiO-67 as novel filler in mixed-matrix membranes for CO2-selective gas separation, J. Membr. Sci. 576 (2019) 78–87.

[20] Y. Jiang, C. Liu, J. Caro, A. Huang, A new UiO-66-NH2 based mixed-matrix membranes with high CO2/CH4 separation performance, Microporous Mesoporous Mater. 274 (2019) 203–211.

[21] M.J.C. Ordonez, K.J. Balkus, J.P. Ferraris, I.H. Musselman, Molecular sieving realized with ZIF-8/Matrimid (R) mixed-matrix membranes, J. Membr. Sci. 361 (2010) 28–37.

[22] J.A. Thompson, J.T. Vaughn, N.A. Brunelli, W.J. Koros, C.W. Jones, S. Nair, Mixed-linker zeolitic imidazolate framework mixed-matrix membranes for aggressive CO2 separation from natural gas, Microporous Mesoporous Mater. 192 (2014) 43–51.

[23] S. Shahid, K. Nijmeijer, Performance and plasticization behavior of polymer-MOF membranes for gas separation at elevated pressures, J. Membr. Sci. 470 (2014) 166–177.

[24] S. Shahid, K. Nijmeijer, S. Nehache, I. Vankelecom, A. Deratani, D. Quemener, MOF-mixed matrix membranes: precise dispersion of MOF particles with better compatibility via a particle fusion approach for enhanced gas separation properties, J. Membr. Sci. 492 (2015) 21–31.

[25] S. Sorribas, B. Zornoza, C. Téllez, J. Coronas, Mixed matrix membranes comprising silica-(ZIF-8) core–shell spheres with ordered meso–microporosity for natural- and bio-gas upgrading, J. Membr. Sci. 452 (2014) 184–192.

[26] Q. Song, S.K. Nataraj, M.V. Roussenova, J.C. Tan, D.J. Hughes, W. Li, P. Bourgoin, M.A. Alam, A.K. Cheetham, S.A. Al-Muhtaseb, E. Sivaniah, Zeolitic imidazolate framework (ZIF-8) based polymer nanocomposite membranes for gas separation, Energy Environ. Sci. 5 (2012) 8359–8369.

[27] R. Castro-Muñoz, V. Fíla, Effect of the ZIF-8 distribution in mixed-matrix membranes based on matrimid® 5218-PEG on CO2 separation, Chem. Eng. Technol. 42 (2019) 744–752.

[28] M. van Essen, E. Montrée, M. Houben, Z. Borneman, K. Nijmeijer, Magnetically aligned and enriched pathways of zeolitic imidazolate framework 8 in Matrimid mixed matrix membranes for enhanced CO2 permeability, Membranes 10 (2020) 155–171.

[29] A. Dhakshinamoorthy, M. Alvaro, Y.K. Hwang, Y.K. Seo, A. Corma, H. Garcia, Intracrystalline diffusion in metal organic framework during heterogeneous catalysis: influence of particle size on the activity of MIL-100 (Fe) for oxidation reactions, Dalton Trans. 40 (2011) 10719–10724.

[30] N. Klein, I. Senkovska, K. Gedrich, U. Stoeck, A. Henschel, U. Mueller, S. Kaskel, A mesoporous metal–organic framework, Angew. Chem. Int. Ed. 48 (2009) 9954–9957.

[31] X. Yan, N. Lu, B. Fan, J. Bao, D. Pan, M. Wang, R. Li, Synthesis of mesoporous and tetragonal zirconia with inherited morphology from metal–organic frameworks, CrystEngComm 17 (2015) 6426–6433.

[32] K. Shen, X. Chen, J. Chen, Y. Li, Development of MOF-derived carbon-based nanomaterials for efficient catalysis, ACS Catal. 6 (2016) 5887–5903.

[33] Y. Chen, J. Wu, W. Yang, Y. Fu, R. Zhou, S. Chen, L. Zhang, Y. Song, L. Wang, Zn/Fe-MOFs-derived hierarchical ball-in-ball ZnO/ZnFe2O4@carbon nanospheres with exceptional lithium storage performance, J. Alloys Compd. 688 (2016) 211–218.

[34] F. Yang, H. Huang, X. Wang, F. Li, Y. Gong, C. Zhong, J.-R. Li, Proton conductivities in functionalized UiO-66: tuned properties, thermogravimetry mass, and molecular simulation analyses, Cryst. Growth Des. 15 (2015) 5827–5833.

[35] D. Qian, C. Lei, G.-P. Hao, W.-C. Li, A.-H. Lu, Synthesis of hierarchical porous carbon monoliths with incorporated metal–organic frameworks for enhancing volumetric based CO2 capture capability, ACS Appl. Mater. Interfaces 4 (2012) 6125–6132.

[36] Y. Mao, D. Chen, P. Hu, Y. Guo, Y. Ying, W. Ying, X. Peng, Hierarchical mesoporous metal–organic frameworks for enhanced CO2 capture, Chem. Eur J. 21 (2015) 15127–15132.

[37] J. Fonseca, S. Choi, Synthesis of a novel amorphous metal organic framework with hierarchical porosity for adsorptive gas separation, Microporous Mesoporous Mater. 310 (2021), 110600.

[38] P.-Q. Liao, D.-D. Zhou, A.-X. Zhu, L. Jiang, R.-B. Lin, J.-P. Zhang, X.-M. Chen, Strong and dynamic CO2 sorption in a flexible porous framework possessing guest chelating claws, J. Am. Chem. Soc. 134 (2012) 17380–17383.

[39] P.-Q. Liao, N.-Y. Huang, W.-X. Zhang, J.-P. Zhang, X.-M. Chen, Controlling guest conformation for efficient purification of butadiene, Science 356 (2017) 1193–1196.

[40] H. Wee Lik, T. Lescouet, J. Ethiraj, F. Bonino, R. Vidruk, E. Garrier, D. Packet, S. Bordiga, D. Farrusseng, M. Herskowitz, A. Martens Johan, Hierarchical zeolitic imidazolate framework-8 catalyst for monoglyceride synthesis, ChemCatChem 5 (2013) 3562–3566.

[41] R.P. Mayer, R.A. Stowe, Mercury porosimetry—breakthrough pressure for penetration between packed spheres, J. Colloid Sci. 20 (1965) 893–911.

[42] S. Shahid, K. Nijmeijer, High pressure gas separation performance of mixed-matrix polymer membranes containing mesoporous Fe(BTC), J. Membr. Sci. 459 (2014) 33–44.

[43] H.-L. Jiang, Y. Tatsu, Z.-H. Lu, Q. Xu, Non-, micro-, and mesoporous Metal−Organic framework isomers: reversible transformation, fluorescence sensing, and large molecule separation, J. Am. Chem. Soc. 132 (2010) 5586–5587.

[44] Y. Yue, Z.-A. Qiao, P.F. Fulvio, A.J. Binder, C. Tian, J. Chen, K.M. Nelson, X. Zhu, S. Dai, Template-free synthesis of hierarchical porous metal–organic frameworks, J. Am. Chem. Soc. 135 (2013) 9572–9575.

[45] M. Eddaoudi, J. Kim, N. Rosi, D. Vodak, J. Wachter, M. O'Keeffe, O.M. Yaghi, Systematic design of pore size and functionality in isoreticular MOFs and their application in methane storage, Science 295 (2002) 469–472.

[46] J. Garcia-Martinez, C. Xiao, A. Cychosz Katie, K. Li, W. Wan, X. Zou, M. Thommes, Evidence of intracrystalline mesostructured porosity in zeolites by advanced gas sorption, electron tomography and rotation electron diffraction, ChemCatChem 6 (2014) 3110–3115.

[47] J. Van Aelst, D. Verboekend, A. Philippaerts, N. Nuttens, M. Kurttepeli, E. Gobechiya, M. Haouas, P. Sree Sreeprasanth, F.M. Denayer Joeri, A. Martens Johan, E.A. Kirschhock Christine, F. Taulelle, S. Bals, V. Baron Gino, A. Jacobs Pierre, F. Sels Bert, Catalyst design by NH4OH treatment of USY zeolite, Adv. Funct. Mater. 25 (2015) 7130–7144.

[48] K. Zhang, R.P. Lively, C. Zhang, R.R. Chance, W.J. Koros, D.S. Sholl, S. Nair, Exploring the framework hydrophobicity and flexibility of ZIF-8: from biofuel recovery to hydrocarbon separations, J. Phys. Chem. Lett. 4 (2013) 3618–3622.

[49] S. Basu, A. Cano-Odena, I.F.J. Vankelecom, MOF-containing mixed-matrix membranes for CO2/CH4 and CO2/N-2 binary gas mixture separations, Separ. Purif. Technol. 81 (2011) 31–40.

[50] J. Cravillon, S. Münzer, S.-J. Lohmeier, A. Feldhoff, K. Huber, M. Wiebcke, Rapid room-temperature synthesis and characterization of nanocrystals of a prototypical zeolitic imidazolate framework, Chem. Mater. 21 (2009) 1410–1412.

[51] R.A. Hayes, Amine-modified Polyimide Membranes, Europen patent EP 0401005, 1990, p. A1.

[52] H. Ren, J. Jin, J. Hu, H. Liu, Affinity between metal-organic frameworks and polyimides in asymmetric mixed matrix membranes for gas separations, Ind. Eng. Chem. Res. 51 (2012) 10156–10164.

[53] I.F.J. Vankelecom, S. Van den broeck, E. Merckx, H. Geerts, P. Grobet, J. B. Uytterhoeven, Silylation to improve incorporation of zeolites in polyimide films, J. Phys. Chem. 100 (1996) 3753–3758.

[54] T.S. Chung, S.S. Chan, R. Wang, Z.H. Lu, C.B. He, Characterization of permeability and sorption in Matrimid/C-60 mixed matrix membranes, J. Membr. Sci. 211 (2003) 91–99.

[55] Q. Yang, C. Zhong, Molecular simulation of carbon dioxide/methane/hydrogen mixture adsorption in metal-organic frameworks, J. Phys. Chem. B 110 (2006) 17776–17783.

[56] D.R. Paul, Gas sorption and transport IN glassy-polymers, Berichte Der Bunsen-Gesellschaft-Phys. Chem. Chem. Phys. 83 (1979) 294–302.

[57] V. Stannett, The transport of gases in synthetic polymeric membranes — an historic perspective, J. Membr. Sci. 3 (1978) 97–115.

[58] T. Visser, M. Wessling, When do sorption-induced relaxations in glassy polymers set in? Macromolecules 40 (2007) 4992–5000.

[59] T. Visser, N. Masetto, M. Wessling, Materials dependence of mixed gas plasticization behavior in asymmetric membranes, J. Membr. Sci. 306 (2007) 16–28.

[60] A. Bos, I.G.M. Punt, M. Wessling, H. Strathmann, CO2-induced plasticization phenomena in glassy polymers, J. Membr. Sci. 155 (1999) 67–78.

[61] S. Shahid, K. Nijmeijer, Matrimid®/polysulfone blend mixed matrix membranes containing ZIF-8 nanoparticles for high pressure stability in natural gas separation, Separ. Purif. Technol. 189 (2017) 90–100.

[62] D.R. Paul, Gas sorption and transport in glassy polymers, Ber. Bunsen Ges. Phys. Chem. 83 (1979) 294–302.

[63] F. Villemot, A. Galarneau, B. Coasne, Adsorption and dynamics in hierarchical metal–organic frameworks, J. Phys. Chem. C 118 (2014) 7423–7433.

[64] L. Zhang, G. Wu, J. Jiang, Adsorption and diffusion of CO2 and CH4 in zeolitic imidazolate framework-8: effect of structural flexibility, J. Phys. Chem. C 118 (2014) 8788–8794.

[65] H.-Y. Zhao, Y.-M. Cao, X.-L. Ding, M.-Q. Zhou, Q. Yuan, Effects of cross-linkers with different molecular weights in cross-linked Matrimid 5218 and test temperature on gas transport properties, J. Membr. Sci. 323 (2008) 176–184.

[66] E.M. Mahdi, J.-C. Tan, Mixed-matrix membranes of zeolitic imidazolate framework (ZIF-8)/Matrimid nanocomposite: Thermo-mechanical stability and viscoelasticity underpinning membrane separation performance, J. Membr. Sci. 498 (2016) 276–290.

[67] C.M. Zimmerman, W.J. Koros, Polypyrrolones for membrane gas separations. II. Activation energies and heats of sorption, J. Polym. Sci. B Polym. Phys. 37 (1999) 1251–1265.

[68] J. Hyo Park, K. Min Choi, H. Joon Jeon, Y. Jung Choi, J. Ku Kang, In-situ observation for growth of hierarchical metal-organic frameworks and their self sequestering mechanism for gas storage, Sci. Rep. 5 (2015), 12045.

[69] T. Rodenas, M. van Dalen, P. Serra-Crespo, F. Kapteijn, J. Gascon, Mixed matrix membranes based on NH2-functionalized MIL-type MOFs: influence of structural and operational parameters on the CO2/CH4 separation performance, Microporous Mesoporous Mater. 192 (2014) 35–42.

[70] T. Rodenas, I. Luz, G. Prieto, B. Seoane, H. Miro, A. Corma, F. Kapteijn, F.X. Llabrés i Xamena, J. Gascon, Metal–organic framework nanosheets in polymer composite materials for gas separation, Nat. Mater. 14 (2015) 48–55.

[71] A. Kılıç, Ç. Atalay-Oral, A. Sirkecioğlu, Ş.B. Tantekin-Ersolmaz, M.G. Ahunbay, Sod-ZMOF/Matrimid® mixed matrix membranes for CO2 separation, J. Membr. Sci. 489 (2015) 81–89.